assembly of TiO_2 particles 20–30 nm diameter in size, that is of highly porous morphology. After annealing at 673 K for 1 h the electrodes were modified with pyrene-functionalized gold nanoparticles by immersing into a THF solution of the nanoparticles overnight. The electrodes were washed thoroughly with THF to remove any unbound gold nanoparticles. These electrodes are referred to as OTE/TiO_2/**1**.

Absorption spectra were recorded with a Shimadzu 3101 spectrophotometer, transmission electron micrographs (TEM) with a Hitachi H600 transmission electron microscope. For the spectroelectrochemical experiments a Princeton applied research model 175 galvanostat/potentiostat was used, details of which can be found elsewhere.[22] The fluorescence from the nanostructured gold film was monitored with an SLM S-8000 photon-counting spectrofluorimeter in a front-face geometry. The other components of the cell were a Pt counter electrode, a saturated calomel reference electrode (SCE) and acetonitrile containing 0.1M tetrabutylammonium perchlorate (TBAP) as electrolyte.

Received: December 27, 2001
Revised: May 6, 2002 [Z18441]

[1] O. V. Makarova, A. E. Ostafin, H. Miyoshi, J. R. Norris, D. Meisel, *J. Phys. Chem. B* **1999**, *103*, 9080.
[2] A. C. Templeton, W. P. Wuelfing, R. W. Murray, *Acc. Chem. Res.* **2000**, *33*, 27.
[3] A. N. Shipway, E. Katz, I. Willner, *PhysChemPhys* **2000**, *1*, 18.
[4] X. M. Zhao, Y. N. Xia, G. M. Whitesides, *J. Mater. Chem.* **1997**, *7*, 1069.
[5] J. J. Hickman, D. Ofer, P. E. Laibinis, G. M. Whitesides, M. S. Wrighton, *Science* **1991**, *252*, 688.
[6] S. Chen, R. S. Ingram, M. J. Hostetler, J. J. Pietron, R. W. Murray, T. G. Schaaff, J. T. Khoury, M. M. Alvarez, R. L. Whetten, *Science* **1998**, *280*, 2098.
[7] R. Elghanian, J. J. Storhoff, R. C. Mucic, R. L. Letsinger, C. A. Mirkin, *Science* **1997**, *277*, 1078.
[8] W. P. McConnell, J. P. Novak, L. C. Brousseau III, R. R. Fuierer, R. C. Tenent, D. L. Feldheim, *J. Phys. Chem. B* **2000**, *104*, 8925.
[9] K. G. Thomas, P. V. Kamat, *J. Am. Chem. Soc.* **2000**, *122*, 2655.
[10] B. I. Ipe, K. G. Thomas, S. Barazzouk, S. Hotchandani, P. V. Kamat, *J. Phys. Chem. B* **2002**, *106*, 18.
[11] S. Chen, R. W. Murray, *J. Phys. Chem. B* **1999**, *103*, 9996.
[12] P. Avouris, B. N. J. Persson, *J. Phys. Chem.* **1984**, *88*, 837.
[13] K. Saito, *J. Phys. Chem. B* **1999**, *103*, 6579.
[14] T. Pagnot, D. Barchiesi, G. Tribillon, *Appl. Phys. Lett.* **1999**, *75*, 4207.
[15] A. C. Templeton, J. J. Pietron, R. W. Murray, P. Mulvaney, *J. Phys. Chem. B* **2000**, *104*, 564.
[16] P. V. Kamat, M. de Lind, S. Hotchandani, *Isr. J. Chem.* **1993**, *33*, 47.
[17] D. Lawless, S. Kapoor, D. Meisel, *J. Phys. Chem.* **1995**, *99*, 10329.
[18] M. Brust, J. Fink, D. Bethell, D. J. Schiffrin, C. Kiely, *J. Chem. Soc. Chem. Commun.* **1995**, 1655.
[19] The oxidation potential of excited pyrene is around -1.5 V versus NHE, which thermodynamically favors transfer of electrons to gold nanoparticles ($E_F = 0.5$ V).
[20] V. Subramanian, E. Wolf, P. V. Kamat, *J. Phys. Chem. B* **2001**, *105*, 11439.
[21] M. Brust, M. Walker, D. Bethell, D. J. Schiffrin, R. Whyman, *J. Chem. Soc. Chem. Commun.* **1994**, 801.
[22] P. V. Kamat, I. Bedja, S. Hotchandani, L. K. Patterson, *J. Phys. Chem. B* **1996**, *100*, 4900.

Valence-Ordering Structures and Magnetic Behavior of Metallic MMX Chain Compounds**

Minoru Mitsumi,* Kouhei Kitamura, Ayumi Morinaga, Yoshiki Ozawa, Mototada Kobayashi, Koshiro Toriumi,* Yasuhito Iso, Hiroshi Kitagawa, and Tadaoki Mitani

Recently, 1D halogen-bridged mixed-valence dinuclear metal complexes, so-called MMX chain compounds, have attracted significant attention as quasi-1D electronic systems characterized by strong electron–phonon, electron–electron, and magnetic interactions. Only two families of MMX chain compounds, namely $[\{A_4[Pt_2(pop)_4X]\cdot n H_2O\}_\infty]$ (pop = $P_2O_5H_2^{2-}$, A = Li, K, Cs, NH_4, X = Cl, Br, I)[1] and $[\{M_2(dta)_4I\}_\infty]$ (dta = $CH_3CS_2^-$, M = Ni, Pt)[2] have been reported. These compounds are 1D chain systems based on a mixed-valence dinuclear unit with a formal oxidation number of +2.5 and a metal–metal bond with a formal bond order of 1/2. An important feature of MMX chain compounds is the increase in internal degrees of freedom upon introducing a dinuclear unit in the mixed-valence state. This property enables a variety of electronic structures, represented by the extreme valence-ordering states shown in Figure 1. These valence-ordering structures would be classified based on the periodicity of the 1D chains as follows. The averaged valence (AV) and charge-polarization (CP) states, in which the periodicity of 1D chains is M-M-X-, correspond to a metallic state with an effective half-filled conduction band mainly composed of M–Mdσ*–Xp_z-hybridized orbitals or to the Mott–Hubbard semiconducting state. In contrast, the periodicity of 1D chains in the charge density wave (CDW) and alternate charge-polarization (ACP) states is doubled, and these electronic structures are regarded as Peierls and spin-Peierls states,[3] respectively.

Kitagawa et al. have reported that $[\{Pt_2(dta)_4I\}_\infty]$ exhibits metallic conducting behavior above 300 K in an AV state.[2d] On the results of a ^{129}I Mössbauer spectroscopic study, the valence-ordering structure of this compound at temperatures

[*] Dr. M. Mitsumi, Prof. Dr. K. Toriumi, K. Kitamura, A. Morinaga, Prof. Dr. Y. Ozawa, Prof. Dr. M. Kobayashi
Department of Material Science
Himeji Institute of Technology
3-2-1 Kouto, Kamigori-cho, Hyogo 678-1297 (Japan)
Fax: (+81) 791-58-0155
E-mail: mitsumi@sci.himeji-tech.ac.jp, toriumi@sci.himeji-tech.ac.jp
Y. Iso, Prof. Dr. H. Kitagawa,[+] Prof. Dr. T. Mitani
Japan Advanced Institute of Science and Technology
Tatsunokuchi, Ishikawa 923-1292 (Japan)
[+] Current address: Department of Chemistry
University of Tsukuba
Tsukuba 305-8571 (Japan)

[**] This work was supported by a Grants-in-Aids for Scientific Research (10740307 and 09440232) and Priority Areas "Metal-Assembled Complexes" (11136244) from the Ministry of Education, Science, Sports and Culture, Japan. M.M. gratefully appreciates Prof. Dr. N. Sakai for use of the SQUID magnetometer. M = metal center, X = halogen.

Supporting information for this article is available on the WWW under http://www.angewandte.org or from the author.

  1433-7851/02/4115-2767 $ 20.00+.50/0

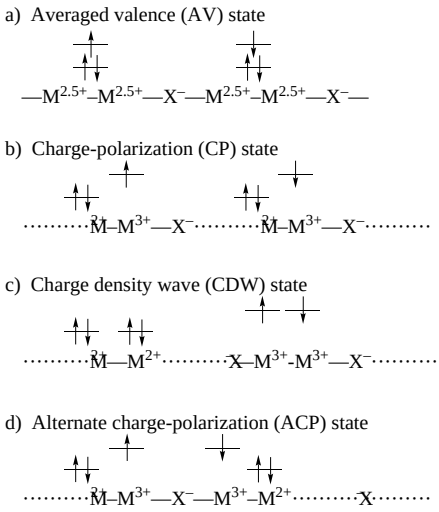

Figure 1. Schematic representation of electronic and lattice structures of the MMX chain compound, where the electrons occupy the Md_{z^2} orbitals.

below 80 K was concluded to be an ACP state. However, no loss in the spin degree of freedom for this system has yet been observed. Recently, we studied the crystal structure and solid-state properties of $[\{Pt_2(EtCS_2)_4I\}_\infty]$, and revealed a metal–semiconductor (M–S) transition at $T_{M-S} = 205$ K, above which the remarkable thermal vibration of a bridging iodine atom in the AV state was observed.[4] This compound shows diffuse scattering corresponding to a twofold repetition length of the Pt-Pt-I- unit above T_{M-S}. Diffuse scattering begins to convert into superlattice reflections below 140 K. These superlattice reflections are considered to have originated from a CDW or ACP state. The spin degree of freedom, however, persisted down to 2 K.

We report the structural phase-transition, valence-ordering structure and magnetic properties of a new metallic MMX chain compound, $[\{Pt_2(n\text{BuCS}_2)_4I\}_\infty]$ (**1**), as well as its transport properties and an efficient chemical synthesis. This compound clearly exhibits an abrupt drop in the magnetic susceptibility, similar to the spin-Peierls transition, accompanying a first-order phase transition at about 210 K. We have also performed a crystal structure analysis of $[\{Pt_2(EtCS_2)_4I\}_\infty]$ (**2**) at 48 K which included superlattice reflections to determine its valence-ordering structure in the low-temperature phase. This work has clarified the correlation between the crystal structures and magnetic properties of **1** and **2**.

Black needle crystals of **1** were grown by the slow cooling of a toluene–*n*-hexane solution of equimolar amounts of $[Pt_2(n\text{BuCS}_2)_4]$ and $[Pt_2(n\text{BuCS}_2)_4I_2]$.[5]

Differential scanning calorimetry (DSC) measurements of **1** were carried out in the temperature range of 153–443 K. Two peaks of latent heat corresponding to the first-order phase transition were observed in the temperature ranges of 204–212 K and 318–323 K, which revealed the existence of three phases, the low-temperature (LT), room-temperature (RT), and high-temperature (HT) phases.

Compound **1** exhibits relatively high electrical conductivity (17–83 $S\,cm^{-1}$) at room temperature, comparable to the conductivity of $[\{Pt_2(dta)_4I\}_\infty]$ (ca. 13 $S\,cm^{-1}$)[2d] and **2** (5–30 $S\,cm^{-1}$).[4] The temperature dependence of electrical resistivity ρ, indicates metallic conduction in the HT phase above the transition temperature, $T_{M-S} = 325$ K. The LT and RT phases show semiconducting behavior with activation energies of 134 and 255 meV, respectively. The thermoelectric power *S*, was also measured in the temperature range of 200–400 K. The HT phase shows almost temperature-independent behavior of S ($-10\,\mu V\,K^{-1}$), which indicates the existence of a half-filled metallic band.[6] Below $T_{M-S} = 325$ K, S slightly decreases with decreasing temperature, and reaches a minimum value of $-16\,\mu V\,K^{-1}$ near 270 K and then, as is characteristic of semiconductors, increases. Furthermore, ρ and S exhibit sharp increases at around 210 K.

ORTEP diagrams of **1** in the RT and LT phases are shown in Figure 2. Compound **1** undergoes a first-order phase-transi-

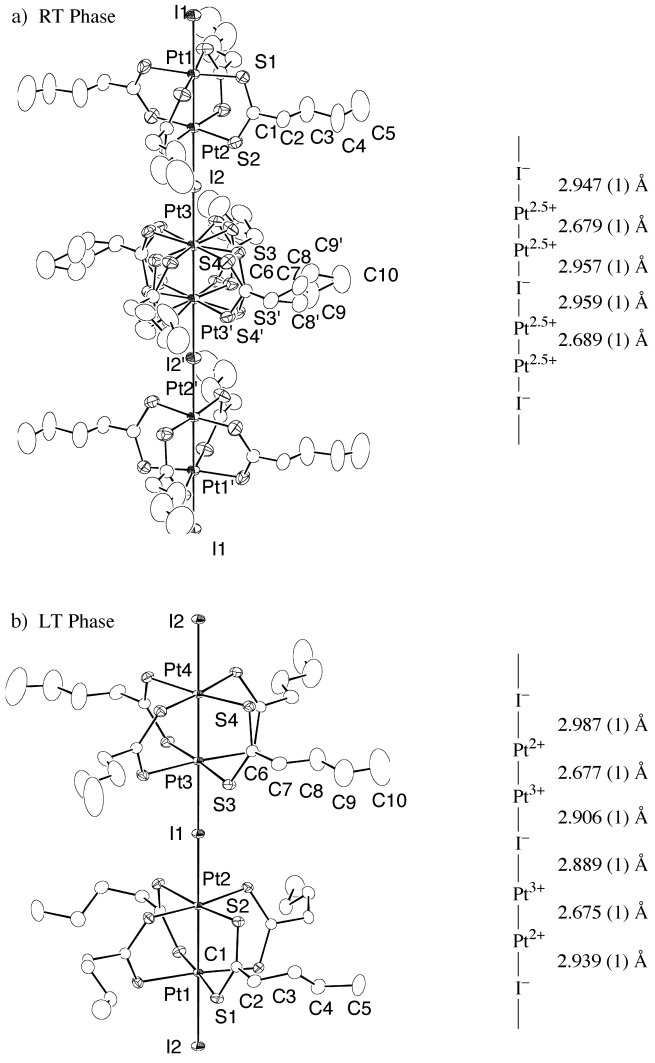

Figure 2. ORTEP diagrams (thermal ellipsoids set at the 50% probability level) and relevant interatomic distances of **1**: a) RT phase (298 K), b) LT phase (167 K).

tion at 204–212 K, where the space group changes from *I*4/*m* in the RT phase to *P*4/*n* in the LT phase. In both phases, the crystal consists of a neutral 1D chain with a Pt-Pt-I- repeating unit lying on the crystallographic fourfold axis parallel to the *c* axis. The periodicity of the crystal lattice in the 1D chain

  1433-7851/02/4115-2768 $ 20.00+.50/0 *Angew. Chem. Int. Ed.* **2002**, *41*, No. 15

direction, however, changes from threefold with a Pt-Pt-I-period in the RT phase to twofold in the LT phase. In the RT phase, all the iodine atoms are located near the midpoint between two diplatinum units and the three crystallographically independent Pt-I bonds are nearly equivalent (2.947 (1), 2.957 (1), and 2.959 (1) Å). Generally, a Pt^{2+}–I^- separation is greater than a Pt^{3+}–I^- separation as the d_{z^2} orbital of a Pt^{2+} site is occupied by a pair of electrons. Therefore, the difference between Pt–I bonds enables us to determine the valence state of Pt atoms. The observed Pt–I bonds indicate a valence-ordering structure close to the AV state. The shortest interchain S···S distance is S2···S2 $(1/2-x,\ 1/2-y,\ 1/2-z) = 5.121(4)$ Å, which indicates the absence of interchain S···S contacts. In the LT phase, however, there are two Pt–I groups. The shortest Pt–I bonds (2.889(1), 2.906(1) Å) are about 0.07 Å shorter than the longest Pt–I bonds (2.939(1), 2.987(1) Å), though the two Pt–Pt bonds are equivalent (2.675(1) and 2.677(1) Å). As judged by Pt–Pt and Pt–I bonds, the valence-ordering structure in the LT phase can be regarded as an ACP state.

To clarify which valence-ordering structure can be adopted in the ground state of **2**, crystal-structure analysis at 48 K was preformed, which included superlattice reflections (Figure 3). When superlattice reflections are included the space group

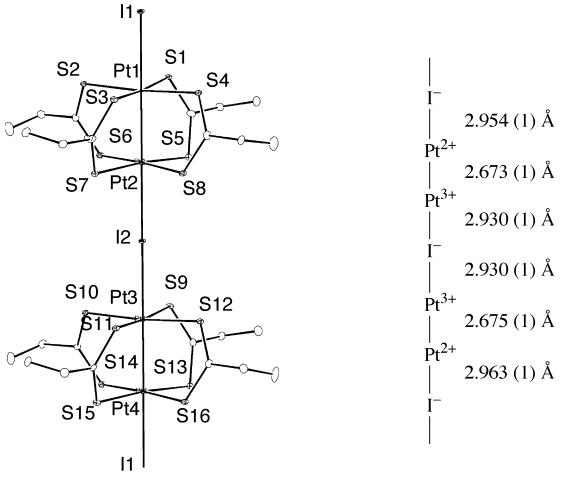

Figure 3. ORTEP diagram (thermal ellipsoids set at the 50% probability level) and relevant interatomic distances of **2** at 48 K.

changes from $C2/c$ to $P\bar{1}$. Periodicity along the 1D chain direction is a twofold Pt-Pt-I- period. Though the two Pt–Pt bonds are equivalent (2.673(1), 2.675(1) Å), the shortest Pt–I distances (2.930(1), 2.930(1) Å) are about 0.02-0.03 Å smaller than the longest Pt–I bonds (2.954(1), 2.963(1) Å). Judging from the Pt–Pt and Pt–I bonds, the valence-ordering structure of **2** at low temperature can be concluded to be an ACP state, similar to the structure of **1** in the LT phase. These valence-ordering structures are consistent with theoretical predictions by Borshch et al. based on semiempirical quantum-chemical band calculations.[7]

The temperature dependence of the magnetic susceptibility χ_M, of crystalline samples of **1** was measured in the temperature range of 5–350 K under a magnetic field H of 1 T. Results are shown in Figure 4, along with those for **2**.[4] The χ_M of **1** in the RT phase is on the order of 2.9×10^{-5} emu mol^{-1}, which is in accordance with results from EPR measurements (ca. 2×10^{-5} emu mol^{-1}).[8] This value is

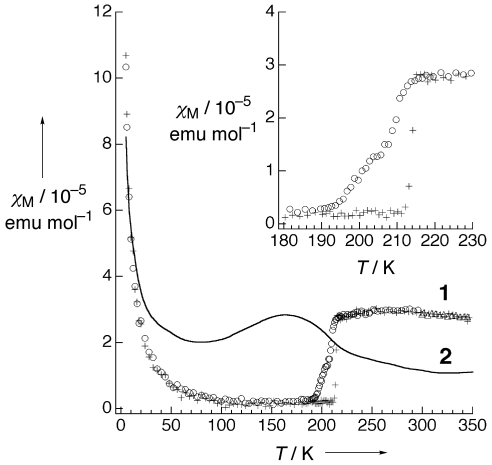

Figure 4. Temperature dependence of the χ_M of **1**: ○ 1st cooling, + 1st heating, △ 2nd cooling (inset expansion between 180 and 230 K); —— magnetic susceptibility of **2**.[4]

smaller by approximately one or two orders of magnitude than those of typical 1D antiferrromagnetic spin systems with $S = 1/2$,[9] which indicates that antiferromagnetic coupling between unpaired electrons on the Pt^{3+} sites is very large. The tail, observed in the χ_M versus T plot below around 30 K, may arise from paramagnetic centers originating from impurities and/or lattice defects. The estimated Curie spin concentration is 0.14%. The most striking feature is an abrupt drop in the χ_M of **1** to the spin-singlet state, with hysteresis, around the first-order phase transition.[10] The electrical and magnetic transitions observed in **1** are similar to *N*-methyl-*N*-ethyl-morpholinium bis-7,7,8,8-tetracyano-*p*-quinodimethanide [MEM(TCNQ)$_2$], which shows two phase transitions, a metal-semiconductor transition at 335 K and a spin-Peierls transition at 19 K.[3] The abrupt drop of χ_M in **1** is quite similar to spin-Peierls transitions. The observed magnetic behavior of **1**, however, seems to be well described not by the spin-Peierls transition, but by the regular electronic Peierls transition. This situation is suggested as the transition is first order in nature, the transition temperature is very high, and sharp increases in ρ and S are observed at the transition. The origin of lattice distortion is attributable to electron–phonon interactions.

χ_M of **2** is of the order of $1-3 \times 10^{-5}$ emu mol^{-1} in the temperature range of 50–350 K (Figure 4).[4] Although the AV to ACP phase transition was observed around $T_{M-S} = 205$ K, an abrupt drop in χ_M has not been observed for **2**, which indicates that the spin degree of freedom persists down to 2 K, similar to $[\{Pt_2(dta)_4I\}_\infty]$.[2d] This quite remarkable difference in the magnetic behaviors of **1** and **2** is attributed to the degree of lattice distortion in the 1D MMX chains, as shown in Figure 5. X-ray crystal structure analyses revealed that differences between Pt^{3+}–I^- and Pt^{2+}–I^- bonds of **1** (ca. 0.07 Å) are remarkably larger than those for **2** (0.02–0.03 Å).

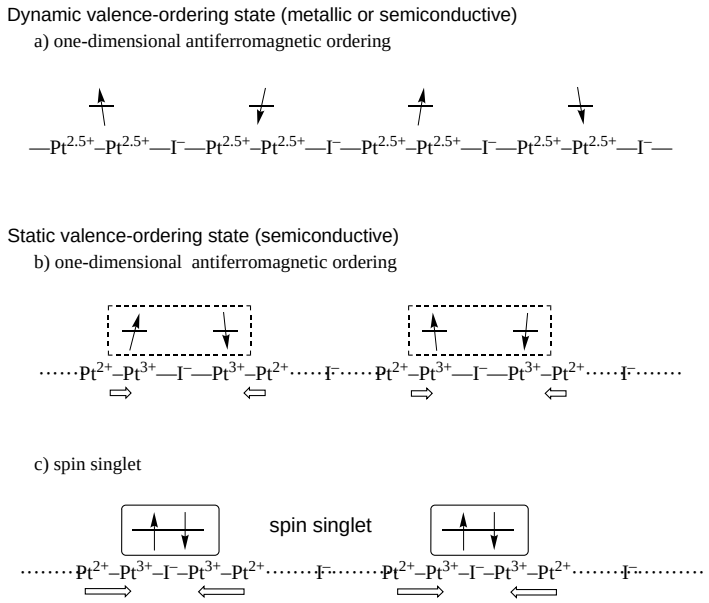

Figure 5. Schematic representation of the valence-ordering and spin states of $[\{Pt_2(RCS_2)_4I\}_\infty]$ (R = *n*Bu (**1**) and Et (**2**)). a) high- and room-temperature phases of **1**, and **2** at room temperature; b) low-temperature phase of **2**; c) low-temperature phase of **1**.

As these distance differences correspond to the lattice distortion of a 1D MMX chain, it is reasonable to consider that the alternation of an exchange interaction in **1** increases with an increase in lattice distortion, resulting in the spin-singlet state of the low-temperature ACP state.

Experimental Section

1: The compounds $[Pt_2(n\text{BuCS}_2)_4]$ (41 mg, 0.044 mmol) and $[Pt_2(n\text{BuCS}_2)_4I_2]$ (52 mg, 0.044 mmol) were dissolved in toluene (3 mL) at 70 °C and then *n*-hexane (4 mL) was added.[5] After being slowly cooled to 2 °C, black needles separated from the solution and were collected by suction filtration and washed with acetone: yield 78 mg (84 %). Elemental analysis (%) calcd for $C_{20}H_{36}IPt_2S_8$: C 22.88, H 3.46; found: C 22.91, H 3.46; UV/Vis/NIR (KBr): $\lambda_{max} = 1110$, 560, 403, 304 nm.

X-ray crystallography for **1** and **2**: Data for **1** were collected at 298 and 167 K on an Enraf Nonius CAD4 diffractometer with graphite-monochromated $Mo_{K\alpha}$ radiation ($\lambda = 0.71069$ Å). A numerical absorption correction was applied to all intensity data. The structures were solved by direct methods (SIR92)[11a] and refined by full-matrix least-squares on F^2 (SHELXL-97).[11b] All calculations were performed with the teXsan crystallographic software package.[11c] Crystal data for **1** at 298 K: $C_{20}H_{36}IPt_2S_8$, $M_r = 1050.07$, black needle, $0.26 \times 0.13 \times 0.12$ mm, tetragonal, space group *I*4/*m*, $a = 13.525(1)$, $c = 25.773(2)$ Å, $V = 4714.4(4)$ Å^3, $Z = 6$, $\rho_{calcd} = 2.219$ g cm^{-3}, $F(000) = 2958$, $\mu(Mo_{K\alpha}) = 10.380$ mm^{-1}, $2\theta_{max} = 59.9°$. 7272 reflections were measured, of which 3512 were unique ($R_{int} = 0.0274$). All non-hydrogen atoms were refined anisotropically. The ligand moiety (S3, S4, C7, and C8) of one of the three diplatinum units in the RT phase is disordered on the mirror plane that is perpendicular to the 1D chain and passes through the midpoint of the Pt3 and Pt3′ atoms. $wR2 = 0.1177$, $S = 1.035$ (all data), $R1$(1710 reflections with $I > 2\sigma(I)$) = 0.0344, 132 parameters, min./max. residual electron density −3.70/0.79 e Å^{-3}, min./max. transmission 0.2577/0.3376. **1** at 167 K: $C_{20}H_{36}IPt_2S_8$, $M_r = 1050.07$, black needle, $0.19 \times 0.14 \times 0.13$ mm, tetragonal, space group *P*4/*n*, $a = 13.419(5)$, $c = 17.072(10)$ Å, $V = 3074(2)$ Å^3, $Z = 4$, $\rho_{calcd} = 2.268$ g cm^{-3}, $F(000) = 1972$, $\mu(Mo_{K\alpha}) = 10.612$ mm^{-1}, $2\theta_{max} = 60.0°$. 4992 reflections were measured, of which 4501 were unique ($R_{int} = 0.046$). All non-hydrogen atoms were refined anisotropically while all hydrogen atoms were placed at their idealized positions. $wR2 = 0.0907$, $S = 1.057$ (all data), $R1$(3209 reflections with $I > 2\sigma(I)$) = 0.0324, 145 parameters, min./max. residual electron density -3.36/1.20 e Å^{-3}, min./max. transmission 0.2482/0.3224.

Crystal data for **2**: $C_{12}H_{20}IPt_2S_8$, $M_r = 937.88$, black plate, $0.20 \times 0.12 \times 0.07$ mm, triclinic, space group $P\bar{1}$, $a = 9.652(1)$, $b = 15.481(1)$, $c = 15.685(1)$ Å, $\alpha = 98.972(2)$, $\beta = 103.516(2)$, $\gamma = 97.610(3)°$, $V = 2215.8(3)$ Å^3, $Z = 4$, $\rho_{calcd} = 2.811$ g cm^{-3}, $F(000) = 1716$, $\mu(0.5609$ Å$) = 7.97$ mm^{-1}, $2\theta_{max} = 60.0°$. Data were collected at 48 K under vacuum (5.5×10^{-4} Pa) using synchrotron radiation (22.10 keV, $\lambda = 0.5609$ Å) and the MAC Science low-temperature vacuum X-ray camera equipped with an imaging plate (IP) area detector at the BL02B1 beamline of the SPring-8 facility. The frames were indexed and the reflections integrated using DENZO and subsequently scaled using SCALEPACK.[12] 20594 unique reflections were measured ($R_{int} = 0.065$). The structure was solved by direct methods (SIR97)[11d] and refined by full-matrix least-squares on F^2 (SHELXL-97).[11b] All calculations were performed with the teXsan crystallographic software package.[11c] $wR2 = 0.1837$, $S = 1.033$ (all data), $R1$(11901 reflections with $I > 2\sigma(I)$) = 0.0537, 415 parameters, min./max. residual electron density −6.780/6.919 e Å^{-3} (peaks are in the vicinity of a Pt1 position). All non-hydrogen atoms were refined anisotropically while all hydrogen atoms were placed at their idealized positions. Crystallographic data (excluding structure factors) for the structures reported in this paper have been deposited with the Cambridge Crystallographic Data Centre as supplementary publication nos. CCDC-177479 – 177481 contains the supplementary crystallographic data for this paper. These data can be obtained free of charge via www.ccdc.cam.ac.uk/conts/retrieving.html (or from the Cambridge Crystallographic Data Centre, 12, Union Road, Cambridge CB2 1EZ, UK; fax: (+44) 1223-336-033; or deposit@ccdc.cam.ac.uk).

Magnetic susceptibility data of **1** was measured using a Quantum Design MPMS-5SH SQUID magnetometer. Correction for core diamagnetism was made using half the sum of the observed diamagnetism for $[Pt_2(n\text{BuCS}_2)_4]$ and $[Pt_2(n\text{BuCS}_2)_4I_2]$. DC electrical conductivity measurements of **1** were made on several single crystals using a four-probe technique. The thermoelectric power was measured through a dynamic differential method using two sets of Au(Fe)-chromel thermocouples (76 μm ∅).

Received: January 17, 2002
Revised: March 19, 2002 [Z 18539]

[1] a) C.-M. Che, F. H. Herbstein, W. P. Schaefer, R. E. Marsh, H. B. Gray, *J. Am. Chem. Soc.* **1983**, *105*, 4604 – 4607; b) M. Kurmoo, R. J. H. Clark, *Inorg. Chem.* **1985**, *24*, 4420 – 4425; c) R. J. H. Clark, M. Kurmoo, H. M. Dawes, M. B. Hursthouse, *Inorg. Chem.* **1986**, *25*, 409 – 412; d) L. G. Butler, M. H. Zietlow, C.-M. Che, W. P. Schaefer, S. Sridhar, P. J. Grunthaner, B. I. Swanson, R. J. H. Clark, H. B. Gray, *J. Am. Chem. Soc.* **1988**, *110*, 1155 – 1162; e) B. I. Swanson, M. A. Stroud, S. D. Conradson, M. H. Zietlow, *Solid State Commun.* **1988**, *65*, 1405 – 1409; f) M. A. Stroud, H. G. Drickamer, M. H. Zietlow, H. B. Gray, B. I. Swanson, *J. Am. Chem. Soc.* **1989**, *111*, 66 – 72; g) M. Yamashita, S. Miya, T. Kawashima, T. Manabe, T. Sonoyama, H. Kitagawa, T. Mitani, H. Okamoto, R. Ikeda, *J. Am. Chem. Soc.* **1999**, *121*, 2321 – 2322.

[2] a) C. Bellitto, A. Flamini, L. Gastaldi, L. Scaramuzza, *Inorg. Chem.* **1983**, *22*, 444 – 449; b) C. Bellitto, G. Dessy, V. Fares, *Inorg. Chem.* **1985**, *24*, 2815 – 2820; c) M. Yamashita, Y. Wada, K. Toriumi, T. Mitani, *Mol. Cryst. Liq. Cryst.* **1992**, *216*, 207 – 212; d) H. Kitagawa, N. Onodera, T. Sonoyama, M. Yamamoto, T. Fukawa, T. Mitani, M. Seto, Y. Maeda, *J. Am. Chem. Soc.* **1999**, *121*, 10068 – 10080.

[3] a) J. W. Bray, L. V. Interrante, I. S. Jacobs, J. C. Bonner in *Extended Linear Chain Compounds*, *Vol. 3* (Ed.: J. S. Miller), Plenum, New York, **1983**, pp. 353 – 415, and references therein; b) M. Kurmoo, M. A. Green, P. Day, C. Bellitto, G. Staulo, F. L. Pratt, W. Hayes, *Synth. Met.* **1993**, *55 – 57*, 2380 – 2385.

[4] M. Mitsumi, T. Murase, H. Kishida, T. Yoshinari, Y. Ozawa, K. Toriumi, T. Sonoyama, H. Kitagawa, T. Mitani, *J. Am. Chem. Soc.* **2001**, *123*, 11179 – 11192.

  1433-7851/02/4115-2770 $ 20.00+.50/0

[5] $[Pt_2(n\text{BuCS}_2)_4]$ and $[Pt_2(n\text{BuCS}_2)_4I_2]$ were prepared by the similar procedures with literature methods using toluene and *n*-hexane.[4]
[6] P. M. Chaikin, R. L. Greene, S. Etemad, E. Engler, *Phys. Rev. B* **1976**, *13*, 1627 – 1632.
[7] S. A. Borshch, K. Prassides, V. Robert, A. O. Solonenko, *J. Chem. Phys.* **1998**, *109*, 4562 – 4568.
[8] H. Tanaka, K. Marumoto, S. Kuroda, M. Mitsumi, K. Toriumi, unpublished results.
[9] O. Kahn, *Molecular Magnetism*, VCH, New York, **1993**, pp. 251 – 286.
[10] Field dependence of χ_M of **1** was also measured near the phase-transition temperature under the magnetic field of $H = 1 - 5$ T. No variation was observed up to 5 T.
[11] a) A. Altomare, G. Cascarano, C. Giacovazzo, A. Guagliardi, M. C. Burla, G. Polidori, M. Camalli, *J. Appl. Crystallogr.* **1994**, *27*, 435 (SIR92); b) G. M. Sheldrick, SHELXL-97, University of Göttingen, Göttingen (Germany), **1997**; c) Crystal Structure Analysis Package, Molecular Structure Corporation, **1985**, **1999**; d) A. Altomare, M. C. Burla, M. Camalli, G. L. Cascarano, C. Giacovazzo, A. Guagliardi, A. G. G. Moliterni, G. Polidori, R. Spagna, *J. Appl. Crystallogr.* **1999**, *32*, 115 – 119 (SIR97).
[12] Z. Otwinowski, W. Minor, *Methods Enzymol.* **1997**, *276*, 307 – 326.

Highly Selective Transport of Organic Compounds by Using Supported Liquid Membranes Based on Ionic Liquids**

Luís C. Branco, João G. Crespo, and Carlos A. M. Afonso*

The selective separation of organic compounds is a critical issue in the chemical industry. In case of readily crystallized molecules, selective crystallization is the most practical method for selective separation, whereas for solutes that are liquid at room temperature, separation by fractional distillation, solvent extraction, or chromatographic methods are more convenient. Some of the above-mentioned methods are technically demanding, involve considerable energy costs, and/or result in large amounts of waste solvents. Membranes, defined as permeable and selective barriers between two phases, have been successfully applied in a large diversity of separation processes, including bioseparations, in which classical separation methods are less convenient, undesirable or even not applicable. The reason for the successful use of membrane-based separation processes stems from the fact that these processes have a high energy efficiency, can be used under moderate temperature and pressure conditions, do not require any additional separating agents or adjuvants, and therefore they are regarded as environmentally friendly.[1] Solute extraction and recovery by using supported liquid membranes is recognized as one of the most promising membrane-based processes. In a supported liquid-membrane system, a defined solvent or solvent/carrier solution is immobilized inside the porous structure of a polymeric or ceramic membrane, which separates the feed phase (in which the solutes of interest are solubilized) from the receiving phase (in which these solutes will be transferred and, eventually, concentrated). This configuration has attracted a great deal of interest because the amount of solvent/carrier needed is minimal, the solvent/carrier is continuously regenerated as a result of solute transport to the receiving phase, and loss of the solvent/carrier phase is negligible if an appropriate supported liquid membrane is designed.[2] The use of a room-temperature ionic liquid (RTIL) as an immobilized phase in the supporting membrane between two organic phases in the feed and the receiving compartments is particularly interesting owing to the nonvolatile character of RTILs and their solubility in the surrounding phases, which allows very stable supported liquid membranes to be obtained without any observable loss of the RTIL to the atmosphere or the contacting phases. Herein we show the potential for continuous separation of organic compounds based on the selective transport through supported liquid membranes that contain RTILs.

RTILs that involve a 1,3-dialkylimidazolium cation are attracting increasing interest as new media, mainly because of the advantage of being nonvolatile. Depending on the anion and on the alkyl group of the imidazolium cation, the RTIL can solubilize supercritical CO_2 ($scCO_2$), a large range of polar and nonpolar organic compounds, and also transition-metal complexes. Simultaneously, they have low miscibility with water, alkanes, and dialkyl ethers[3] and are insoluble in $scCO_2$.[4] As a result of these properties, they are emerging as an alternative recyclable, environmentally benign, reaction medium for chemical transformations, including transition-metal catalysis[3] and biocatalysis.[3f, 5] Their use has also been successfully extended as a potential stationary phase for gas chromatography,[6] in pervaporation,[7] and for the substitution of traditional organic solvents (OS) in aqueous – OS[7a, 8] and OS – $scCO_2$ biphasic extractions.[4, 9] It is assumed that the 1,3-dialkylimidazolium RTIL are not a statistical aggregate of anions and cations, but instead a more organized structure that contains polar and nonpolar regions as a result of the formation of weak interactions, mainly as hydrogen bonds, with 2-H of the imidazolium ring.[10] The above information prompted us to study the potential of using RTIL in supported liquid membranes for selective separation processes.

To illustrate the concept, and as a result of transport studies with representative organic functional compounds, we used a mixture of the organic isomeric amines hexylamine, diisopropylamine, and triethylamine (1:1:1 molar ratio) in diethyl ether in side A of the cell (Figure 1). The two sides of the cell were separated by the RTIL 1-*n*-butyl-3-methylimidazolium hexafluorophosphate ([bmim][PF_6]) immobilized in the por-

[*] Prof. C. A. M. Afonso, L. C. Branco, Prof. J. G. Crespo
Departamento de Química, Centro de Química Fina e Biotecnologia
Faculdade de Ciências e Tecnologia, Universidade Nova de Lisboa
2829-516 Caparica (Portugal)
Fax: (+351) 21-294-8550
E-mail: cma@dq.fct.unl.pt

[**] This work was supported by the European Commission (contract QLK3-CT-1999-01213) and the Fundação para a Ciência e Tecnologia (project PRAXIS/C/QUI/10069/98). We also acknowledge Raquel Fortunato for the technical support with the membranes and for helpful discussions.

  1433-7851/02/4115-2771 $ 20.00+.50/0